SMALL-SIZE WWAN HANDSET ANTENNA DISPOSED AT A SMALL NOTCH IN THE SYSTEM GROUND PLANE

Kin-Lu Wong, Yeh-Chun Kao, and Fang-Hsien Chu
Department of Electrical Engineering, National Sun Yat-Sen University, Kaohsiung 804, Taiwan; Corresponding author: wongkl@ema.ee.nsysu.edu.tw

Received 20 January 2012

ABSTRACT: *An internal WWAN (824–960/1710–2170 MHz) handset antenna suitable to be disposed at a small notch of 35 × 6 mm^2 in the system ground plane of the handset is presented. Also, the antenna has a low profile of 3 mm above the main circuit board on which the system ground plane is printed. That is, the antenna occupies a small volume of 35 × 6 × 3 mm^3 or 0.63 cm^3 only (much less than 1 cm^3). To fit in the small notch, a quarter-wavelength gap-coupled loop antenna is applied, which not only can be configured into a compact configuration but also can be in proximity to the surrounding ground plane. With the aid of a matching network, which is comprised of a series chip inductor and a band-stop matching circuit, two wide operating bands to, respectively, cover the GSM850/900 and GSM1800/1900/UMTS operation are obtained. Details of the proposed antenna are described. The applied techniques in achieving wideband operation with a small antenna size are discussed.* © 2012 Wiley Periodicals, Inc. Microwave Opt Technol Lett 54:2498–2503, 2012; View this article online at wileyonlinelibrary.com. DOI 10.1002/mop.27125

Key words: *mobile antennas; handset antennas; WWAN antennas; loop antennas; coupled-fed loop antennas*

1. INTRODUCTION

For internal handset antenna applications, the loop antenna has the attractive feature of closed resonant path, which makes it promising to be in proximity to nearby ground plane such that there is no significant coupling in between the loop strip and the ground plane to degrade the antenna performance. This feature is advantageous for the loop antenna over the traditional monopole antenna or inverted-F antenna to be in compact integration inside the handset [1, 2]. However, the loop antenna is normally operated at its half-wavelength resonant mode as the lowest mode, when it is placed nearby and connected to the system ground plane of the handset. The nearby connected ground plane makes it possible for the loop antenna to generate its unbalanced half-wavelength resonant mode, in addition to its balanced one-wavelength mode. Several internal loop antennas operated at its half-wavelength resonant mode for the WWAN operation in the handset have also been reported [3–10]. However, if the internal loop antenna can be operated at its quarter-wavelength mode, like the traditional monopole antenna or inverted-F antenna operated at its quarter-wavelength mode [11], it is expected that the occupied volume of the loop antenna inside the handset can be further decreased.

Recently, the quarter-wavelength loop antennas suitable for the handset applications have also been demonstrated [1, 2, 12–14]. By applying a coupling feed [1, 2, 12, 13] or loading a series chip capacitor at the feeding point [14], a quarter-wavelength mode of the loop antenna can be generated. In these studies, the required length of the loop strip is much less than those of the traditional half-wavelength loop antennas [3–10]. The occupied volume of these quarter-wavelength loop antennas inside the handset is hence decreased [1, 2, 12–14]. It is also noted that the loop antenna studied in [1] is shown to be in close proximity to a protruded ground extended from the system ground plane. Because associated electronic elements can be accommodated on the protruded ground, compact integration of the internal antenna inside the handset can thereby be obtained.

In this article, we demonstrate a promising quarter-wavelength loop antenna suitable to be disposed at a small notch of 35 × 6 mm^2 (210 mm^2) in the system ground plane of the handset for the WWAN operation in the 824–960 and 1710–2170 MHz bands. The required clearance or no-ground region for the proposed antenna in the system ground plane is 210 mm^2 only, much less than 15 × 25 mm^2 (375 mm^2) in [1] or 10 × 40 mm^2 (400 mm^2) in [13]. Further, the clearance region is a small notch at the center of the bottom edge of the system ground plane, similar to that in [13], but different from that in [1], which is at one of the corners of the system ground plane.

To fit in the small notch of 35 × 6 mm^2, the proposed loop antenna applies a gap-coupled loop strip, which is configured into a compact configuration showing a low profile of 3 mm above the main circuit board of the handset. That is, the antenna volume is 35 × 6 × 3 mm^3 (0.63 cm^3) only. The coupling gap is disposed close to the feeding point of the antenna, which leads to the generation of a quarter-wavelength loop mode at about 850 MHz for the antenna's lower band. With the aid of a matching network formed by a series chip inductor and a band-stop circuit, the bandwidth of the antenna's lower band can be greatly enhanced. The matching network can also improve the bandwidth of the antenna's upper band, which is formed by the higher-order modes of the loop antenna.

The proposed loop antenna has a simple structure and can be easily fabricated at low cost. Detailed operating principle of the proposed antenna is addressed in the article. Results of the fabricated prototype including its far-field radiation characteristics are also presented. Near-field radiation characteristics such as the specific absorption rate (SAR) [15, 16] and hearing aid compatibility (HAC) [17–19] are also analyzed.

2. PROPOSED ANTENNA

Figure 1(a) shows the geometry of the proposed WWAN handset antenna disposed at a small notch in the system ground plane, and the dimensions of the antenna's metal pattern are given in Figure 1(b). To show the proposed antenna more clearly, photos of the fabricated prototype are shown in Figure 2. The small notch of size 35 × 6 mm^2 is at the center of the bottom edge of the system ground plane, which is printed on a 0.8-mm thick FR4 substrate of size 60 × 115 mm^2, relative permittivity 4.4, and loss tangent 0.024. The FR4 substrate is treated as the main circuit board of the handset. To simulate the handset casing, a plastic casing fabricated by a 1-mm thick plastic slab of relative permittivity 3.0 and loss tangent 0.02 is used in this study. The total thickness of the plastic casing is 10 mm, which is reasonable for modern slim handsets.

The antenna is mainly a gap-coupled loop strip as shown in Figure 1(b). The total length of the loop strip is about 84 mm from point A to D, which is close to about 0.25 wavelength of the frequency at 850 MHz. The loop strip is formed by two portions, the first one (section AB and CD) printed inside the small notch of the main circuit board and the second one (section BC) mounted above the small notch. Section BC is fabricated from cutting a 0.2-mm thick copper plate and connected to the printed portion at point B and C. The total volume of the antenna is 35 × 6 × 3 mm^3 or 630 mm^3 only, and shows a low profile of 3 mm above the main circuit board. Section BC also uses a widened section of width 6 mm, which can improve the impedance matching of the antenna and enhance the operating bandwidth.

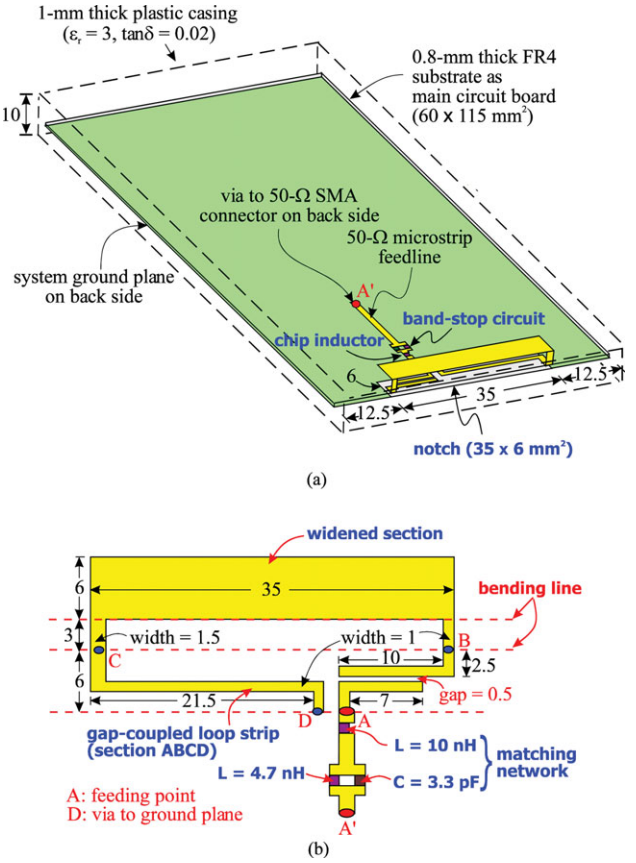

Figure 1 (a) Geometry of the proposed WWAN handset antenna disposed at a small notch in the system ground plane. (b) Dimensions of the antenna's metal pattern. [Color figure can be viewed in the online issue, which is available at wileyonlinelibrary.com]

On the printed portion of the loop strip, there is a coupling gap of 0.5 mm and length 7 mm, which can have a similar behavior of the series chip capacitor in the external matching circuit in [14] and can lead to the generation of a quarter-wavelength loop mode at about 850 MHz in the proposed design. The gap-coupled design is simpler than that in [14] to excite a quarter-wavelength loop mode and is easy to fabricate at low cost. One end (point A) of the printed portion is the antenna's feeding point, while the other end (point D) is grounded to the system ground plane through a via-hole in the main circuit board.

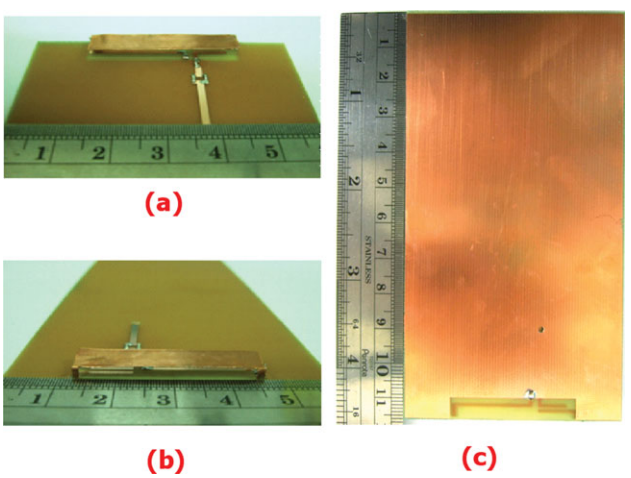

Figure 2 Photos of the fabricated antenna disposed at the bottom edge of the system ground plane. (a) Front view seeing from antenna's feeding point. (b) Front view seeing from bottom edge of the system ground plane. (c) Back view of the system ground plane. [Color figure can be viewed in the online issue, which is available at wileyonlinelibrary.com]

By further adding a matching network comprising a series chip inductor (L = 10 nH in this study) and a band-stop circuit (L = 4.7 nH and C = 3.3 pF), the antenna can provide two wide operating bands for the GSM850/900 and GSM1800/1900/UMTS operation. The wide lower band is obtained by an additional resonant mode contributed by the band-stop circuit [9] and occurred at about 950 MHz to combine with the quarter-wavelength loop mode. In contrast, it is interesting to note that the series chip inductor can lead to good excitation of a higher-order or quarter-wavelength loop mode at about 2000 MHz, which further becomes a dual-resonance mode owing to the presence of the series chip inductor. The dual-resonance quarter-wavelength loop mode forms the wide upper band for the antenna. Details of the proposed matching network on enhancing the antenna's operating bandwidth will be discussed with the aid of Figures 6 and 7 in section 3. Also note that, with the proposed matching network, no extra metal strips providing additional resonant paths to generate new resonant modes for the antenna are required. This makes it promising for the proposed antenna to achieve a decreased size yet wideband or multiband operation.

3. RESULTS OF PROPOSED ANTENNA

The antenna was fabricated, and the results of the measured and simulated return loss are shown in Figure 3. The desired operating bands (824–960 and 1710–2170 MHz) are shown in the shaded regions in the figure. Based on 3:1 VSWR definition, which is widely used as the design specification of the internal WWAN handset antenna, the obtained bandwidths cover the desired operating bands. Good agreement between the measurement and the simulation obtained using the three-dimensional full-wave electromagnetic field simulator HFSS version 12 [20] is also seen. Note that in both the lower and upper bands, the wide bandwidths are obtained owing to two resonant modes excited. This behavior can be seen more clearly from the simulated input impedance of the antenna shown in Figure 4. In the lower band, the first mode is identified as a quarter-wavelength loop mode of the antenna (see the surface current distribution at

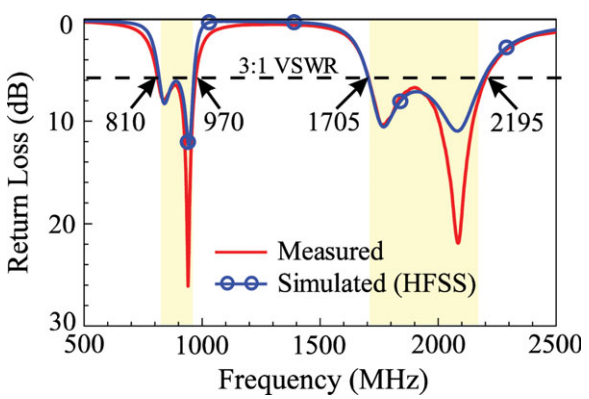

Figure 3 Measured and simulated return loss of the proposed antenna. [Color figure can be viewed in the online issue, which is available at wileyonlinelibrary.com]

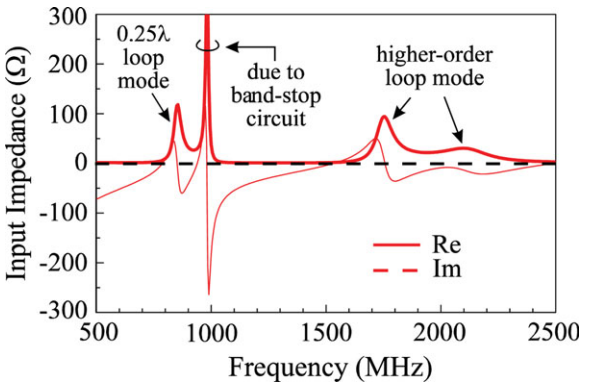

Figure 4 Simulated input impedance of the proposed antenna. [Color figure can be viewed in the online issue, which is available at wileyonlinelibrary.com]

850 MHz shown in Fig. 5), while the second one is owing to a new resonance at about 1020 MHz generated by a parallel resonance at about 1080 MHz contributed by the band-stop circuit [9, 21]. In the upper band, the two resonant modes are higher-order loop modes of the antenna, which are both identified as half-wavelength loop modes (one current null in the current distribution) as seen from the simulated surface current distributions at 1770 and 2080 MHz seen in Figure 5. Hence, the two resonant modes can also be described as a dual-resonance half-wavelength loop mode in the proposed design.

To analyze the operating principle of the antenna more clearly, Figure 6 shows the simulated return loss for the proposed antenna, the corresponding direct-feed loop antenna (Ant1), the case with the gap-coupled loop antenna only (Ant2), and the Ant2 with the chip inductor only (Ant3). It is clearly seen that only when the gap-coupled loop antenna is applied (Ant2 and Ant3), the 0.25-wavelength loop mode at about 850 MHz can be generated. With the chip-inductor loading (Ant3), improved impedance matching of the quarter- and half-wave-

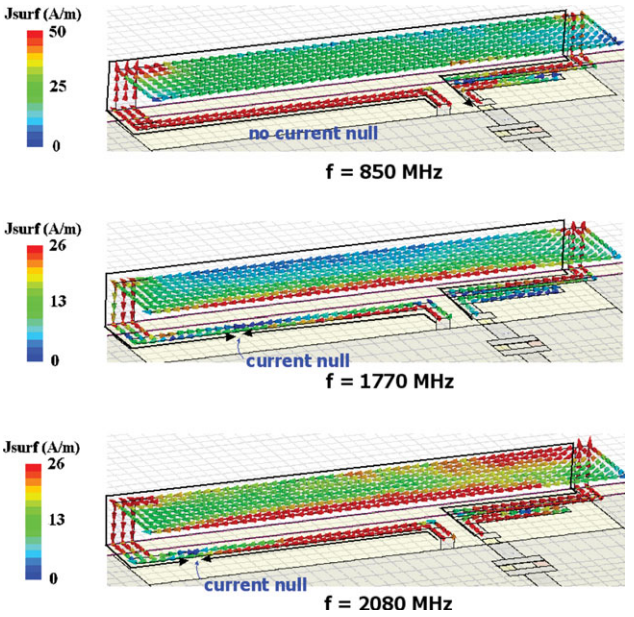

Figure 5 Simulated surface current distributions on the antenna's metal pattern at 850, 1770, and 2080 MHz. [Color figure can be viewed in the online issue, which is available at wileyonlinelibrary.com]

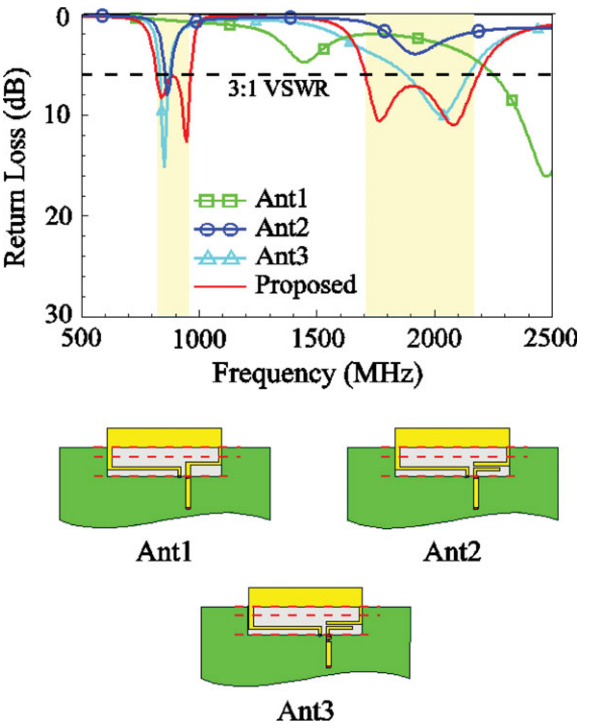

Figure 6 Simulated return loss for the proposed antenna, the corresponding direct-feed loop antenna (Ant1), the case with the gap-coupled loop antenna only (Ant2), and the Ant2 with the chip inductor only (Ant3). [Color figure can be viewed in the online issue, which is available at wileyonlinelibrary.com]

length loop modes is obtained. This behavior can be explained more clearly from the simulated input impedance for Ant2 and Ant3 shown in Figure 7. By further with the presence of the band-stop circuit (proposed antenna), an additional mode occurred at frequencies close to 850 MHz is generated and the half-wavelength mode in the desired upper band also becomes a dual-resonance mode as described in Figure 5.

Figure 8 shows the measured antenna efficiency, which includes the mismatching loss, of the proposed antenna. Over the lower and upper bands, the antenna efficiency varies from about 50–65% and 52–85%, respectively. The measured three-dimensional (3D) total-power radiation patterns of the antenna are shown in Figure 9. The side view of the full 3D patterns and the cross-sectional view at the *x-z* plane at five

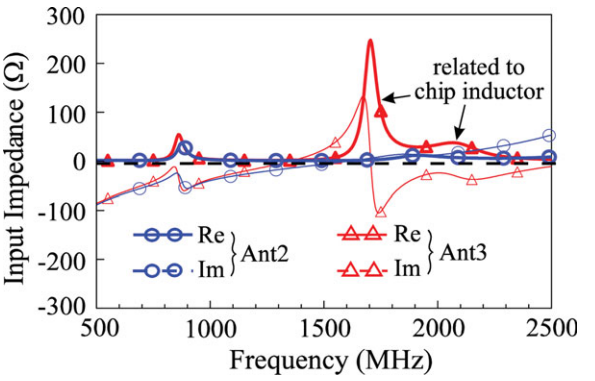

Figure 7 Simulated input impedance for the Ant2 and Ant3 studied in Fig. 6. [Color figure can be viewed in the online issue, which is available at wileyonlinelibrary.com]

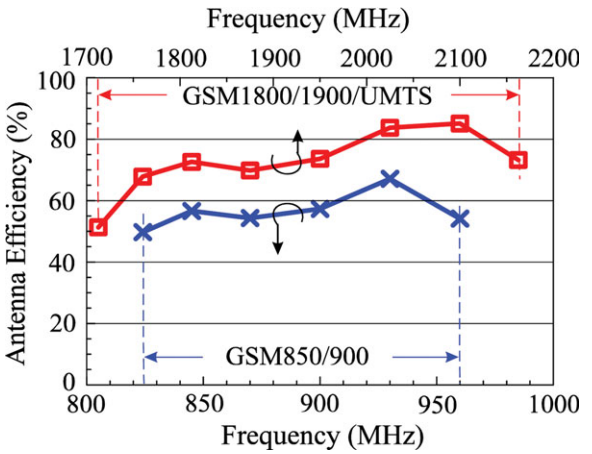

Figure 8 Measured antenna efficiency (mismatching loss included) of the proposed antenna. [Color figure can be viewed in the online issue, which is available at wileyonlinelibrary.com]

representative frequencies are presented. At 859 and 925 MHz (central frequencies of the GSM850 and GSM900 bands), dipole-like patterns with omnidirectional radiation in the azimuthal plane (*x*-*y* plane) are observed. At 1795, 1920, and 2045 MHz (central frequencies of the GSM1800, GSM1900, and UMTS bands), near-omnidirectional radiation in the *x*-*y* plane is still seen. This behavior is attractive for practical applications in achieving good coverage in the azimuthal direction.

With good far-field radiation characteristics obtained, the near-field radiation of the antenna is then studied. The SAR

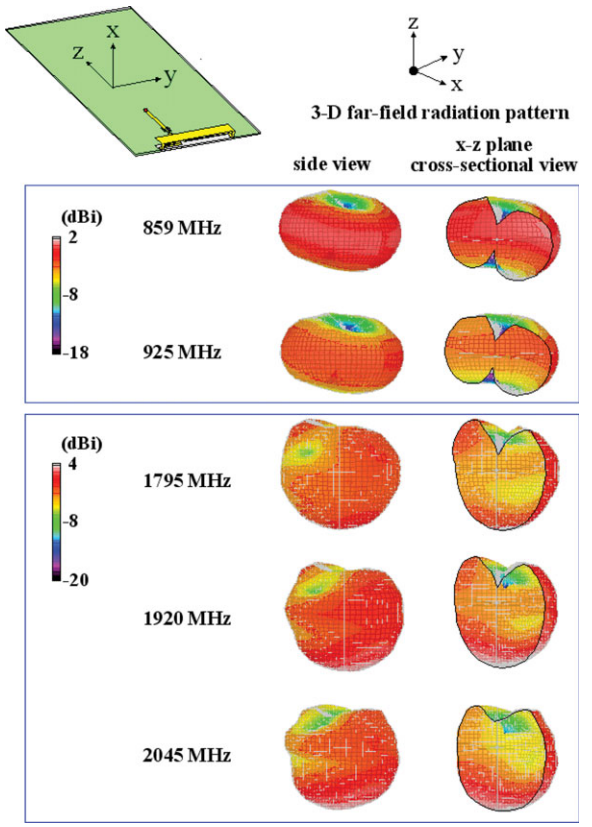

Figure 9 Measured three-dimensional total-power radiation patterns of the proposed antenna. [Color figure can be viewed in the online issue, which is available at wileyonlinelibrary.com]

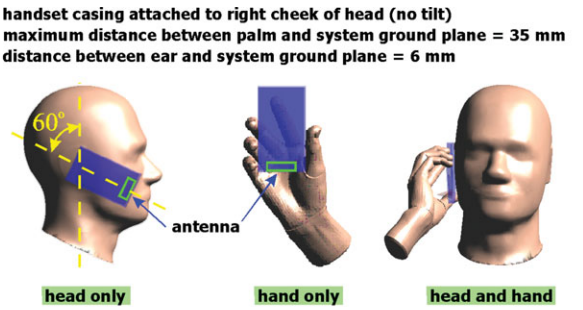

Frequency (MHz)		859	925	1795	1920	2045
1-g SAR (W/kg)	head only	0.78	0.96	0.47	0.44	0.38
	hand only	0.89	1.12	1.84	1.41	1.26
	head and hand	0.96 (0.73)*	1.13 (0.85)*	1.66 (0.48)*	1.45 (0.37)*	1.38 (0.26)*
10-g SAR (W/kg)	head only	0.58	0.73	0.31	0.30	0.27
	hand only	0.58	0.59	1.22	0.95	0.84
	head and hand	0.56 (0.56)*	0.66 (0.66)*	1.26 (0.32)*	0.93 (0.25)*	0.88 (0.18)*
Return loss (dB)	head only	5.9	7.3	6.7	6.7	9.3
	hand only	6.6	6.9	8.5	7.1	7.6
	head and hand	5.9	6.8	8.4	6.0	5.2
	free space	6.1	7.4	7.3	6.7	8.7
Antenna Efficiency (%)	head only	15.6	18.1	35.3	42.8	54.3
	hand only	27.2	28.2	34.7	35.1	38.2
	head and hand	5.4	5.6	10.1	11.3	13.5
	free space	64.9	56.7	65.8	67.5	76.5

( )*: SAR values occurred at the head for the head and hand condition

Figure 10 SAR simulation model and the simulated SAR values. [Color figure can be viewed in the online issue, which is available at wileyonlinelibrary.com]

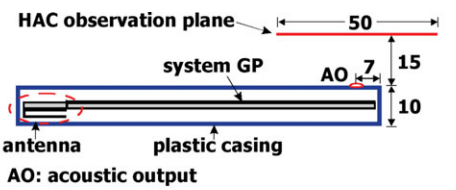

Frequency (MHz)	859	925	1795	1920	2045
E-field (dB)	46.1 (M3)	46.4 (M3)	36.3 (M3)	35.3 (M3)	25.2 (M4)
E-field, M3 limit (dB)	48.5	48.5	38.5	38.5	41.0
H-field (dB)	-9.7 (M4)	-8.6 (M4)	-14.3 (M3)	-15.2 (M3)	-24.8 (M4)
H-field, M3 limit (dB)	-1.9	-1.9	-11.9	-11.9	-9.4
Return loss (dB)	6.1	7.4	7.3	6.7	8.7
Input power (W)	2.0	2.0	1.0	1.0	0.125

Note: M4 limit is 5 dB lower than M3 limit

Figure 11 HAC simulation model and the simulated HAC results. [Color figure can be viewed in the online issue, which is available at wileyonlinelibrary.com]

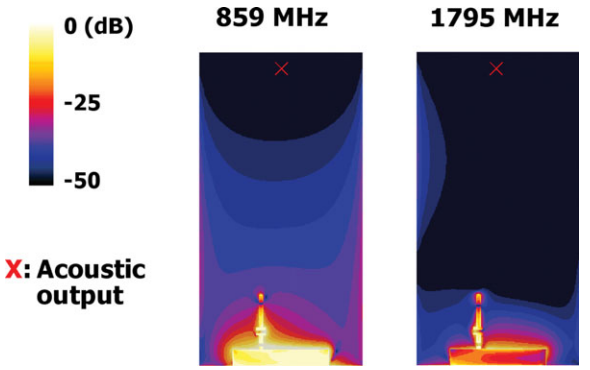

Figure 12 Simulated surface current distributions on the system ground plane at 859 and 1795 MHz. [Color figure can be viewed in the online issue, which is available at wileyonlinelibrary.com]

results of the antenna are first analyzed. Figure 10 shows the SAR simulation model and the simulated SAR values. Three models of the head only, the hand only, and the head and hand-based on the SPEAG simulation software SEMCAD X version 14 [22] are shown in the figure. The handset with the antenna disposed therein is attached to right cheek of the phantom head with no tilt. The orientation of the handset with respect to the phantom head is indicated in the simulation models. The 1-g and 10-g SAR values at five representative frequencies are shown. The obtained 10-g SAR values are all less than the limit of 2.0 W/kg [16]. For considering the SAR values occurred in the phantom head only, which is required in practical SAR testing, the obtained 1-g SAR values are also all less than the limit of 1.6 W/kg [15]. Note that the SAR values in the parentheses in the head and hand condition are the SAR occurred at the head. The obtained SAR results indicate that the proposed antenna is promising for practical handset applications. In Figure 10, the simulated antenna efficiency for free space and three simulation models is also shown for comparison. The low antenna efficiency for the head and hand condition is mainly because there is large power absorption by the very lossy head and hand in close proximity to the handset.

The HAC results are also analyzed. Figure 11 shows the HAC simulation model based on the SEMCAD X version 14 [22] and the simulated HAC results. The near-field E-field and H-field strengths at the observation plane 15 mm above the acoustic output of the handset are all categorized to be M3 or M4 as shown in the figure. That is, the handset with the proposed antenna disposed therein can be treated as an HAC handset [22]. The good behavior of the HAC results is related to the excited surface currents on the system ground plane of the handset as shown in Figure 12, in which it is seen that the surface currents are attracted close to the notch. This makes the excited surface currents weaker near the acoustic output, such that decreased near-field radiation can be obtained at the HAC observation plane.

4. CONCLUSION

An internal WWAN handset antenna with a small volume of 35 $\times$ 6 $\times$ 3 mm^3 (630 mm^3) to cover the 824–960 and 1710–2170 MHz bands has been proposed. The antenna can be in close proximity to the surrounding ground, making it suitable to be disposed in a small notch of 35 $\times$ 6 mm^2 (210 mm^3) at the system ground plane of the handset. The antenna also shows good far-field radiation characteristics and decreased near-field radiation. The proposed antenna is obtained by applying the design techniques of using a quarter-wavelength gap-coupled loop strip with a matching network comprising a series chip inductor and a band-stop circuit. The decreased near-field radiation makes the antenna easy to meet the SAR and HAC requirements for practical handset applications.

REFERENCES

1. K.L. Wong, W.Y. Chen, and T.W. Kang, On-board printed coupled-fed loop antenna in close proximity to the surrounding ground plane for penta-band WWAN mobile phone, IEEE Trans Antennas Propagat 59 (2011), 751–757.
2. F.H. Chu and K.L. Wong, Internal coupled-fed dual-loop antenna integrated with a USB connector for WWAN/LTE mobile handset, IEEE Trans Antennas Propagat 59 (2011), 4215–4221.
3. B. Jung, H. Rhyu, Y.J. Lee, F.J. Harackiewwicz, M.J. Park, and B. Lee, Internal folded loop antenna with tuning notches for GSM/GPS/DCS/PCS mobile handset applications, Microwave Opt Technol Lett 48 (2006), 1501–1504.
4. Y.W. Chi and K.L. Wong, Compact multiband folded loop chip antenna for small-size mobile phone, IEEE Trans Antennas Propagat 56 (2008), 3797–3803.
5. C.I. Lin and K.L. Wong, Internal multiband loop antenna for GSM/DCS/PCS/UMTS operation in the small-size mobile phone, Microwave Opt Technol Lett 50 (2008), 1279–1285.
6. K.L. Wong and C.H. Huang, Printed loop antenna with a perpendicular feed for penta-band mobile phone application, IEEE Trans Antennas Propagat 56 (2008), 2138–2141.
7. Y. W. Chi and K. L. Wong, Half-wavelength loop strip fed by a printed monopole for penta-band mobile phone antenna, Microwave Opt Technol Lett 50 (2008), 2549–2554.
8. H. Rhyu, J. Byun, F.J. Harackiewicz, M.J. Park, K. Jung, D. Kim, N. Kim, T. Kim, and B. Lee, Multi-band hybrid antenna for ultra-thin mobile phone applications, Electron Lett 45 (2009), 773–774.
9. Y.W. Chi and K.L. Wong, Very-small-size folded loop antenna with a band-stop matching circuit for WWAN operation in the mobile phone, Microwave Opt Technol Lett 51 (2009), 808–814.
10. C.W. Chiu, C.H. Chang, and Y.J. Chi, A compact folded loop antenna for LTE/GSM band mobile phone applications, Presented at the 2010 International Conference on Electromagnetics in Advanced Applications (ICEAA), Sydney, Australia, pp. 382–385.
11. K.L. Wong, Planar antennas for wireless communications, Wiley, New York, 2003.
12. Y.W. Chi and K.L. Wong, Quarter-wavelength printed loop antenna with an internal printed matching circuit for GSM/DCS/PCS/UMTS operation in the mobile phone, IEEE Trans Antennas Propagat 57 (2009), 2541–2547.
13. F.H. Chu and K.L. Wong, Internal coupled-fed loop antenna integrated with notched ground plane for WWAN operation in the mobile handset, Microwave Opt Technol Lett 54 (2012), 599–605.
14. Y.W. Chi and K.L. Wong, Very-small-size printed loop antenna for GSM/DCS/PCS/UMTS operation in the mobile phone, Microwave Opt Technol Lett 51 (2009), 184–192.
15. American National Standards Institute (ANSI), Safety levels with respect to human exposure to radio-frequency electromagnetic field, 3 kHz to 300 GHz, ANSI/IEEE standard C95.1, April 1999.
16. IEC 62209-1, Human exposure to radio frequency fields from hand-held and body-mounted wireless communication devices—Human models, instrumentation, and procedures—Part 1: Procedure to determine the specific absorption rate (SAR) for hand-held devices used in close proximity to the ear (frequency range of 300 MHz to 3 GHz), Feb. 2005.
17. American National Standard for Method of Measurement of Compatibility between Wireless Communication Devices and Hearing Aids (ANSI C63.19-2007, revision ANSI C63.19-2006), American National Standards Institute, New York, 2007.
18. T. Yang, W.A. Davis, W.L. Stutzman, and M.C. Huynh, Cellular-phone and hearing-aid interaction: An antenna solution, IEEE Antennas Propagat Mag 50 (2008), 51–65.

19. K.L. Wong and M.F. Tu, Hearing aid-compatible internal penta-band antenna for clamshell mobile phone, Microwave Opt Technol Lett 51 (2009), 1408–1413.
20. http://www.ansys.com/products/hf/hfss/, ANSYS HFSS.
21. K.L. Wong, W.J. Wei, and L.C. Chou, WWAN/LTE printed loop antenna for tablet computer and its body SAR analysis, Microwave Opt Technol Lett 53 (2011), 2912–2919.
22. http://www.semcad.com, SPEAG SEMCAD, Schmid & Partner Engineering AG.

ON THE BENDING EFFECTS ON ARTIFICIAL MAGNETIC CONDUCTORS

Haider R. Khaleel, Hussain M. Al-Rizzo, and Daniel G. Rucker
Department of Systems Engineering, University of Arkansas at Little Rock Little Rock, AR 72204; Corresponding author: hrkhaleel@ualr.edu

Received 21 January 2012

ABSTRACT: *In this letter, we present the performance of a typical artificial magnetic conductor (AMC) under different bending extents. Square patch array-based AMC is employed as a benchmark to demonstrate the dependence of AMC characteristics on the degree of curvature. We show that increasing the extent of bending leads to a shift to a higher resonance frequency and bandwidth degradation which suggests the importance of such analysis when designing AMC structures for conformal applications. Finite element method full wave electromagnetic solver has been employed to extract the reflection phase profile of the structure under study. To the best of the authors' knowledge, this kind of study is being reported for the first time.* © 2012 Wiley Periodicals, Inc. Microwave Opt Technol Lett 54:2503–2505, 2012; View this article online at wileyonlinelibrary.com. DOI 10.1002/mop.27124

Key words: *artificial magnetic conductor (AMC); frequency selective surface (FSS); bending*

1. INTRODUCTION

Artificial magnetic conductors (AMCs) have attracted a great deal of interest in the recent years due to their potential applications in the fields of antennas and microwave circuits [1, 2]. It is well known that a perfect electric conductor (PEC) has a reflection phase of 180° for a plane wave incident, while a perfect magnetic conductor (PMC), which does not exist in nature, has a reflection phase of 0°. AMC, which was first proposed by Seivenpiper [3], can be engineered to resemble PMC, that is, to have in-phase reflection properties in a specified frequency band. These artificial structures are typically realized by a planar periodic metallic pattern often called frequency selective surfaces (FSS), deposited/printed on top of a grounded substrate. AMC surfaces exhibit fascinating properties which can be very beneficial to antennas and microwave circuits. For example, in the field of microstrip antennas, PMC ground planes can be used instead of traditional PECs; as it will ensure in phase image currents and hence, constructive interaction which in turn yields a better antenna efficiency and gain. In-phase reflection can be obtained in PEC ground planes if separated by $\lambda/4$ from the radiator which yields to impractical/high profile systems [4]. Hence, serious efforts were dedicated for the analysis and optimization of AMC structures [5, 6].

Wearable and conformal antenna systems are becoming extremely popular nowadays [7, 8]. Moreover, the integration of AMC structures with such systems is a growing field of research [9, 10]. Textile materials, flexible substrates, and planar structure are normally used to integrate antennas into garment or nonplanar surfaces. In Ref. 10–12, several wearable antennas for WLAN, GPS, telemedicine, and bluetooth applications were studied. One of the main challenges of such systems is the uncertainty of keeping the wearable/conformal antenna system flat during operation especially for elements made of flexible materials. Therefore, it is necessary to evaluate the performance of the antennas and any type of integrated structures under bending conditions. Most previous research was only focused on investigating the bending effects on wearable/conformal antennas based on conventional PEC ground planes both numerically and experimentally [9, 13]. To the best of the authors' knowledge, no research has been reported yet on the performance of AMC structures under bending conditions.

In this letter, we particularly consider the performance of the square patch array FSS-based AMC under different bending extents. The surface impedance of bended AMC structures is modeled in section 1. Structure modeling along with the necessary numerical setup for both flat and bended cases are introduced in Section 3. The performance of the considered AMC structure under different extents of bending is discussed in Section 4. Finally, we conclude the letter in section 5.

2. SURFACE IMPEDANCE OF BENDED SQUARE PATCH ARRAY BASED AMC

The AMC under study (unit cell is shown in Fig. 1) comprises an array of square metallic patches (capacitive grids) positioned on a metal-backed dielectric slab with a thickness h and a relative permittivity εr.

According to Ref. 14, the surface impedance is characterized by the so called ''grid impedance,'' which relates the electric field's tangential component in the grid plane to the induced surface current density by the incident plane wave which flows along the patch grid. The total surface impedance Z_T of this combination could be modeled as a parallel connection of the capacitive grids impedance Z_G and the grounded substrate surface impedance Z_S as in Eq. (1):

$$Z_T^{-1} = Z_G^{-1} + Z_S^{-1} \tag{1}$$

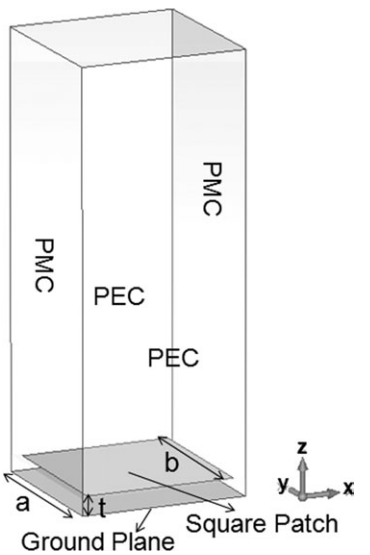

Figure 1 Numerical setup for a square patch unit cell (flat case)